Progress In Electromagnetics Research, Vol. 119, 239–252, 2011

ELECTROMAGNETIC SCATTERING AND DOPPLER ANALYSIS OF THREE-DIMENSIONAL BREAKING WAVE CRESTS AT LOW-GRAZING ANGLES

C. Qi[1], Z. Zhao[1,*], W. Yang[1], Z. Nie[1], and G. Chen[2]

[1]School of Electronic Engineering, University of Electronic Science and Technology of China, Chengdu 610054, China

[2]School of Communication and Information Engineering, Chongqing University of Posts and Telecommunications, Chongqing 400065, China

Abstract—The electromagnetic scattering of the synthesized three-dimensional (3-D) breaking wave crests which are formed by azimuthally aligning the individual 2-D breaking wave profiles has been numerically studied at the low-grazing angles (LGA) by using the multilevel fast multipole algorithm (MLFMA) with adaptive higher order hierarchical Legendre basis functions. Different from the specular (or quasi-specular) reflection and Bragg scattering, the "sea-spike" phenomenon which is characterized by that horizontally polarization (HH) signals greatly exceed vertically polarization (VV) signals has been demonstrated by analyzing both the backscattering of 3-D LONGTANK series and a plunging breaker. For the time-dependent evolution of the plunging breaker, the Doppler shifts and Doppler splitting effects are investigated by applying the fast Fourier transform (FFT) with a moving Hamming window. The spectrum of HH scattering has the feature of concentration, while the spectrum of VV scattering shows the Doppler splitting effects.

1. INTRODUCTION

Electromagnetic (EM) scattering of sea surface is very important in microwave remote sensing. The scattering of breaking waves is regarded as one of the most difficult problems in this field. Numerous studies have been performed on breaking waves [1–4]. When the jets

Received 24 June 2011, Accepted 25 July 2011, Scheduled 1 August 2011

* Corresponding author: Zhiqin Zhao (zqzhao@uestc.edu.cn).

form, the backscattering from the breaking wave crests is considered as the main contribution of the "sea-spike" phenomenon which is characterized by that horizontally polarization (HH) signals exceed the vertically polarization (VV) signals by as much as 10 dB or more at the low-grazing angles (LGA). Therefore, the specular (or quasi-specular) reflection and Bragg scattering are not able to describe the mechanism. Multipath model was introduced by Wetzel [5] to explain the "sea-spike" phenomenon. The main idea of this model is that steep features on the crests of breaking waves are the dominant scatterers, and some energy scatters directly back to the radar from the front face, while some scatters toward the front face of the wave and reflects toward the radar. Trizna [6] refined this model to the finite conductivity of the sea surface. Near the Brewster angle of the sea surface, the multipath of VV is greatly attenuated; leading to HH cross-sections are greater than VV. West introduced another model in [7]. The back reflections from the specular points on the forming jet and within the cavity under the jet can simultaneously add destructively at VV and constructively at horizontal, leading to HH exceeds VV.

Two-dimensional (2-D) numerical investigation of breaking waves has been investigated by West et al. [2, 3]. The scattering of 2-D surfaces representing the time evolution of breaking waves was calculated by using a 2-D hybrid technique combining the method of moment and geometrical theory of diffraction (MoM/GTD). Doppler shifts [8] of the 2-D plunging breaker were studied, showing the Doppler splitting phenomenon around the portion of jets. However, all the above simulations are based on the 2-D model which is regarded as non-real in engineering. Compared with the 2-D model in the previous work, the synthesized 3-D models will be more useful in engineering.

In the research of electromagnetic simulations of the breaking water waves, how to build a reliable computational approach is critical, especially for the scattering at the LGA. Some classical analytical methods, such as the Kirchhoff approximation (KA) [9–11], small perturbation method (SPM) [12, 13] and the two scale model (TSM) [14, 15], cannot work well in the three-dimensional (3-D) sea surface model. In this paper, a numerical method, the multilevel fast multipole algorithm (MLFMA) [16–18] with adaptive higher order hierarchical Legendre basis functions [19] is applied to calculate the scattering at the LGA. The method has the advantages of obtaining the accurate results with the low computational costs in the electromagnetic simulations of the breaking waves.

Using the rigorous numerical method, the electromagnetic scattering of two typical 3-D breaking wave crests, the LONGTANK

series [20] and the measured 2-D plunging breaker [21], is studied by azimuthally aligning the individual 2-D breaking wave crest to synthesize the 3-D sea surface model. It needs to be noted that this method of generating a 3-D model is different from the method used by West [22], where a 3-D model was formed by combining all profiles in the azimuthal direction with a specific spatial interval. In this paper, we synthesize the 3-D model by uniformly extending the each 2-D profile in the azimuthal direction, and each of which represents the evolution history of the breaking waves.

In this paper, the backscattering of 3-D breaking waves is obtained at different incident angles from 60° to 90°. The backscattering data of the 3-D models demonstrate the special "sea-spike" phenomenon for the VV and HH polarizations during the breaking wave process. Moreover, the activity of the synthesized 3-D breaking wave crests is more energetic than the 2-D cases, which can be found in the previous work [21]. The Doppler shifts of the backscattering from the 3-D models in the whole evolution history are studied by applying the fast Fourier transform (FFT) with a time-moving Hamming window. The features of the spectrum for HH and VV are analyzed.

2. BREAKING WAVE CRESTS

In the oceanic engineering, usually the breaking wave crests are obtained through two ways, numerical simulation and experimental measurement. In these studies, the LONGTANK series obtained by numerical simulation and the plunging breaker obtained by experimental measurement are considered as typical models and have been widely used in the electromagnetic analysis of breaking waves. Therefore, they are briefly introduced and discussed in this section. Meanwhile, in order to obtain the 3-D models, the necessary treatments for the original 2-D models have also been presented.

2.1. LONGTANK Series

Wang et al. have developed a two-dimensional numerical wave tank, called LONGTANK wave (it is also called Tulin wave) [20]. The complete time evolution process of the crest is shown in Figure 1. A total of 18 profiles are plotted to describe the gradually developing water breaker. At the beginning, there is no evident breaking portion in the first profile, whereas in the last stage, there is already a jet formed in the 18th profile. These profiles exhibit a gradual steepening of the wave and the formation of a jet.

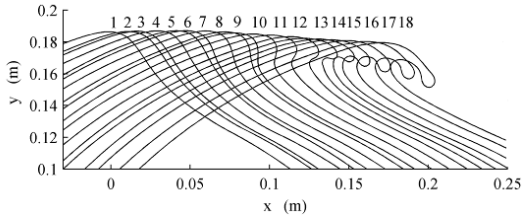

Figure 1. LONGTANK wave profiles.

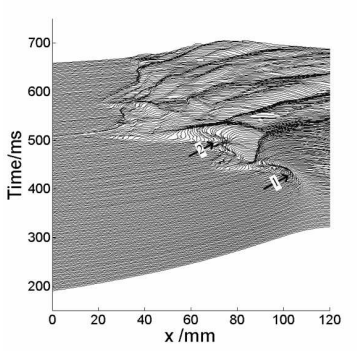

Figure 2. Plunging wave profiles.

2.2. Plunging Breaker

Figure 2 shows a plunger breaker. The wave was mechanically generated in a deep wave tank in the Univ. of Maryland. A total of 222 frames (profile 90 to profile 311) are corresponding to a time history from 190 ms to 659 ms. There are two overturning jets (point 1 and point 2 in this figure) which impact at approximate 360 ms and 460 ms. Smaller steep features have appeared around the jets. After the beginning of breaking, turbulent cells are shed from the crest that is carried by the orbital motion of the wave, which is called as the turbulent "scar". More details about how to obtain the profiles were described in [21].

Considering the edge effects induced by artificially truncation, some specific edge treatments are applied. The 3-D model of the sea surface is developed from the 2-D model as shown in Figure 3. Here, take the 14th profile of the LONGTANK series as an example. First, the planar sections of surfaces angled at 30° down from the horizon are joined at the end of each profile, so that all the points on the extension are shadowed from all points on the rough surface.

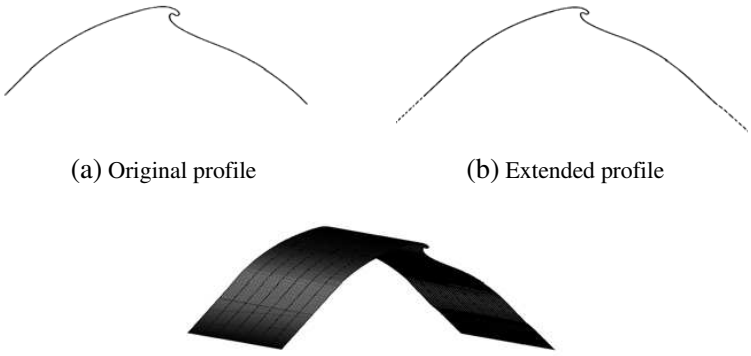

(a) Original profile (b) Extended profile

(c) The 3-D surface model

Figure 3. The generation of 3-D surface (the 14th profile of the LONGTANK series).

The planar sections provide regions for adding resistive loading area. Second, the 3-D profiles used here are formed by extending the 2-D profile uniformly 6λ in the azimuthal direction, so that illumination windows can be added in this direction.

Gaussian window and Thorsos window [23] are two typical illumination windows commonly used to suppress the edge diffraction. Zhao and West introduced a resistive loading approach in the study of 2-D and 3-D breaking waves [24]. The resistive loading method is suitable for plane wave illumination at the LGA. In this paper, two different edge-treatment approaches are used to suppress the edge effects. The resistive loading [25] is applied to the forward and trailing edges of the surface in the range direction, while Gaussian illumination weighting is applied in the azimuthal direction.

3. ELECTROMAGNETIC APPROACH

For electromagnetic scattering, the sea water is considered as dielectric medium. The equivalent impendent boundary condition [19] is used to deal with the boundary scattering. The electric equivalent surface current $\mathbf{J}$ and equivalent magnetic current $\mathbf{M}$ satisfy $\mathbf{n}' \times \mathbf{M} = Zs\mathbf{J}$, where Zs is the surface impedance of the sea water. Zs relates to the electromagnetic frequency, the temperature and the salinity of the ocean water. At 10 GHz, $Zs = 43.92 + i * 13.29\,\Omega$ ($i = \sqrt{-1}$), when the temperature is 20°C and the salinity is 32.54‰.

For the scattering of the rough sea surface, the electric field

integral equation (EFIE) in the Cauchy principal value sense is considered.

$$\mathbf{E}^i_{\tan} = \left[jk\eta \int_s \left\{\mathbf{J} + \frac{1}{k^2}\nabla' \cdot \mathbf{J}\nabla\right\} G ds'\right]_{\tan} + \left[\frac{1}{2} Zs\mathbf{J} + \int_s Zs(\mathbf{n}' \times \mathbf{J}) \times \nabla G ds'\right]_{\tan}, \quad (1)$$

where $\mathbf{E}^i_{\tan}$ is the tangential element of incident electric field, $\mathbf{n}'$ is the outer normal vector of the sea surface, k is the wave number, η is the intrinsic impedance (120π for free space), and G is the Green's function of free space e^{-jkR}/R with $R = |\mathbf{r} - \mathbf{r}'|$.

The MLFMA has been widely used to solve above equation efficiently. In the process of MLFMA, the interactions between the elements are classified as near-region and the far-region. The near-region matrix elements are calculated directly using MoM, while the far-region elements are solved by using MLFMA.

$$\sum_n Z_{mn} a_n = \sum_{n \in NR} Z_{mn} a_n + \sum_{n \in FR} Z_{mn} a_n, \quad (2)$$

where NR represents the near-region and FR represents the far-region, n and m are the number of the testing basis function and source basis function, respectively. a_n are the expansion coefficients needed to solve using the linear matrix equation, and Z_{mn} are the elements of the impedance matrix.

Based on the geometrical feature and electromagnetic property, the higher order hierarchical Legendre vector basis functions has been applied to solve the problem, which can greatly reduce the unknowns and sparsification of the impedance matrix and improve the condition number of the matrix, thus leading to a further reduction of memory and CPU time [19]. In modeling the backscattering from the 3-D breaking wave profiles, this adaptive higher order basis functions can be very effective.

The higher order hierarchical Legendre basis functions are defined on the curvilinear quadrilateral with a curved second-order nine-node model in this paper. The scatterer is meshed using curved quadrilaterals of arbitrary order with associated parametric curvilinear coordinate systems defined by $-1 \leq u,\ v \leq 1$. $\mathbf{r}$ is the source vector defined by the sub-coordinate systems u and v. And the surface current on each patch can be described as

$$\mathbf{J}(\mathbf{r}) = \mathbf{J}(u, v) = I^u \frac{\partial \mathbf{r}}{\partial u} + I^v \frac{\partial \mathbf{r}}{\partial v}, \quad (3)$$

which can be expanded as

$$\mathbf{J}(u,v) = \frac{1}{\eta_s(u,v)} \left\{ \mathbf{u} \sum_{m=0}^{M_u} \sum_{n=0}^{N_v} b_{mn}^u \tilde{C}_m \tilde{P}_m(u) C_n P_n(v) + \mathbf{v} \sum_{m=0}^{M_v} \sum_{n=0}^{N_u} b_{mn}^v \tilde{C}_m \tilde{P}_m(v) C_n P_n(u) \right\} \quad (4)$$

where $\eta_s(u,v)$ is the Jacobian factor, b_{mn}^u and b_{mn}^v are the unknown coefficients, M_u and N_v are the basis orders along the **u**-directed current flow direction and the transverse direction, respectively; M_v and N_u are the basis orders along the **v**-directed current flow direction and the transverse direction, respectively. $\tilde{P}_m(u)$ or $\tilde{P}_m(v)$ are the modified polynomials, which can be defined as (taking the u variable as an example),

$$\tilde{P}_m(u) = \begin{cases} 1-u, & m=0 \\ 1+u, & m=1 \\ P_m(u) - P_{m-2}(u), & m \geq 2 \end{cases}, \quad (5)$$

where $P_m(u)$ and $P_n(v)$ are the expansion polynomials, $\tilde{C}_m$ and C_n are the scaling factors and are defined as

$$\tilde{C}_m = \begin{cases} \frac{\sqrt{3}}{4}, & m=0,1 \\ \frac{1}{2}\sqrt{\frac{(2m-3)(2m+1)}{2m-1}}, & m \geq 2 \end{cases}, \quad (6)$$

$$C_n = \sqrt{n+\frac{1}{2}}, \quad (7)$$

Duffy transform is applied to tackle the singularity of integration between the basis functions and the Green's function.

4. ELECTROMAGNETIC CALCULATIONS

When the incident angle tends to grazing, the multipath effect in the scattering will be evident. This is illustrated in Figure 4. The back reflections from the specular points on the forming jet and within the

Figure 4. Multipath effect of the LONGTANK series (14th profile).

cavity under the jet can simultaneously add destructively at VV and constructively at horizontal, leading to HH exceeds VV.

As mentioned, the MLFMA with adaptive higher order hierarchical Legendre basis functions introduced in Section 3 is applied to calculate the backscattering of breaking waves. Flexible order setting is an important factor in the higher order hierarchical Legendre vector basis functions. The basic idea can be summarized as that once the segmentation is set, the order of the basis functions at different areas can be flexibly adjusted according to its current distribution, which is very effective to analyze the scattering problem of the asymmetric current distribution. Considering the geometry feature and electromagnetic scattering property of breaking waves, different orders of basis function are applied in different portions. The shadowed area and the smooth area will be solved with the n order basis, while the breaking portion will be calculated with the m order basis, which is called as n_m order basis strategy in the paper. Obviously, m is set to be larger than n. How to choose the orders of the basis function has a great impact on the efficiency of MLFMA. Subject to the length of paper, the discussions about the basis strategy can be found in the literature [19]. The 2_3 order is an optimal choice with respect to breaking wave crests. Therefore, MLFMA with 2_3 order basis functions is applied in the all the experiments of breaking waves.

4.1. "Sea-spike" Phenomenon

At the LGA, since the multipath effect between breaking portion and the bottom of crests has occurred, the HH to VV radar cross section (RCS) ratios become unequal or larger for the LGA cases. This behavior is not consistent with the Bragg mechanism, which predicts approximately constant scattering over time with VV significantly exceeding HH. The following two examples of the backscattering of breaking wave crests can verify this phenomenon.

First, the LONGTANK series representative of the whole evolution history are taken into account. As shown in Figure 5, at the moderate incident angles, the multipath effect is very weak, the spike action is not obvious from the monostatic Radar echo with electromagnetic simulation at 60° incident angle. As the incident angle tends to grazing (e.g., 80°), the multipath effect becomes dominate in the scattering mechanism, leading to the HH polarization exceeds the VV polarization, even up to 10 dB. Accordingly, the "sea-spike" phenomenon becomes evident during the jet formation.

Then, the 3-D plunging breaker is studied as the second experiment to demonstrate this phenomenon. There are two overturnings (noted as point 1 and point 2 in Figure 2) in the evolution

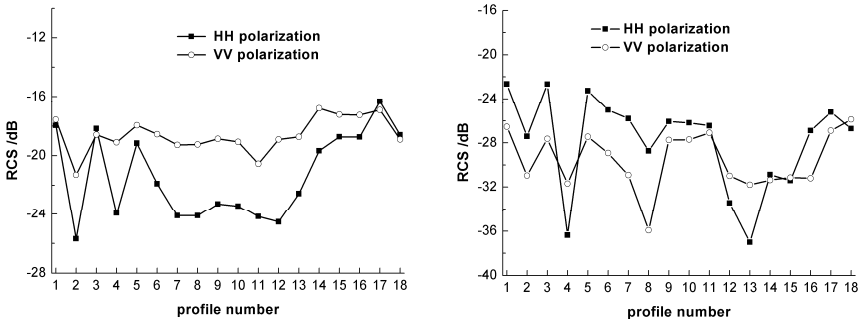

(a) 60° (b) 80°

Figure 5. The backscattering of the LONGTANK series.

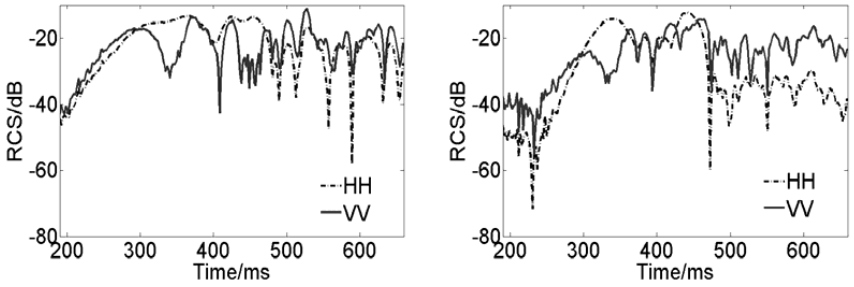

(a) 60° (b) 80°

Figure 6. The backscattering of plunging breaker.

history. The backscattering of plunging breaker is also computed at the incident angles of 60° and 80° respectively, as shown in Figure 6. Through the experiment, "sea-spike" phenomena occurred, which can be clearly distinguished during the formation of the two overturnings at the two incident angles. In the beginning, the plunging breaker is relatively smooth, the wave crest is round and the cross-sections are small. The multipath effects are not dominated (where $VV > HH$). As the crest getting steeper, the cross-sections become larger, at the same time, the multipath effects become more serious than before. The HH exceeds VV, and the "sea-spike" phenomenon appears. When the first large overturning occurs around 360 ms, this phenomenon is so obvious that the HH-to-VV ratio even is up to 20 dB. After the first overturning, the surface turns to calm before the second large overturning occurs, accordingly the "sea-spike" phenomena disappear,

$VV > HH$ once more. However, sea spikes are identified as soon as the second overturning occurs (about at the time of 460 ms), giving HH-to-VV ratios of 10 dB. After the breaking, the activity of the surface is no longer energetic. Meanwhile, the multipath effects are not as serious as before, the "sea-spike" phenomena disappear, and VV exceeds HH again.

4.2. The Doppler Analysis

Except the "sea-spike" phenomena aforementioned, in the time-evolving plunging breaker waves, the phase velocity of the underlying waves in the grow-up and destruction process is greatly different. Therefore, the fast moving surface scatterers are associated with the "fast" scattering, while the lower shifted sea surface scatterers are referred to as "slow" scattering.

In our experiments, the backscattering echoes for the all synthesized 3-D models are applied to analyze the Doppler shifts. The time-dependent Doppler shifts of the plunging breaker are demonstrated by applying a moving Hamming window (with equivalent time resolution of 80 ms) to the continuous backscatter and applying the fast-Fourier transform (FFT). Figures 7 and 8 show the results of the Doppler shifts at the 60° and 80° for two polarizations.

For the HH polarizations at the two incident angles, the strongest Doppler response occurs at 340 ms and 440 ms, with a shift of 220 Hz. They correspond to the maximum velocities of the tip of the two jets. For the VV polarization, the first response occurs at the 300 ms, and then this response quickly decreases to a minimum at the 340 ms. The second strong response is associated with the steep features appearing

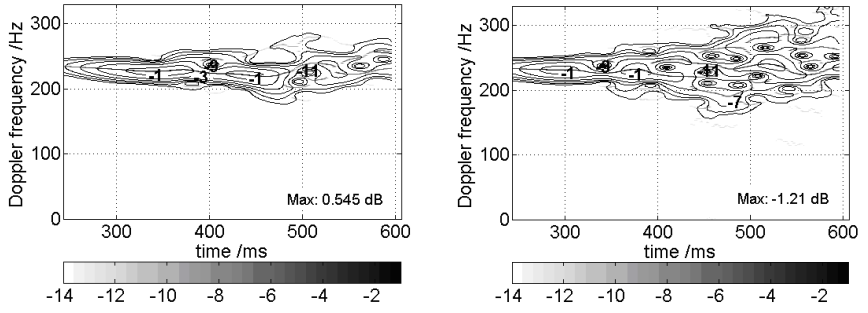

(a) HH (b) VV

Figure 7. The Doppler shifts at 60° incident angle.

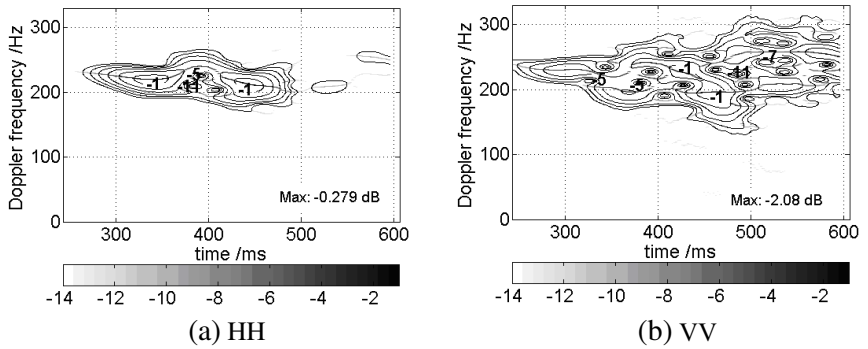

(a) HH (b) VV

Figure 8. The Doppler shifts at 80° incident angle.

from 360 ms to 430 ms. At the 80° incident angle, the strongest Doppler response occurs from 410 ms to 460 ms and gives the shifts ranging from 180 Hz to 230 Hz. In all cases, the echoes with shifts correspond to the velocities correlated with the steep or reentrant features in the grow-up and destruction history of breaking waves. Within the simulations, the maximum Doppler values for two incident angles are presented in Figures 7 and 8. It is shown the HH polarization is higher (about 1.7 dB) than the VV polarization at the moment of sea spikes.

At the LGA (for example, 80°), because the back reflections from the convex jetting region of the wave and the concave cavity region under the jet interfere destruct at VV polarization, the echoes for the VV polarization become more sophisticate than that for HH cases in the whole history. Therefore, the "Doppler splitting" effects have appeared, its spectrum disperses at a much wider bandwidth frequency ranging 150 Hz to 310 Hz. While for the HH cases, the Doppler spectrum appears closer to the frequency associated with the phase velocity of the breaking waves.

This is a little different from the 2-D simulation result given by Zhao and West [24] that predicts Doppler splitting phenomenon using MoM/GTD. It mainly due to that in the 2-D simulation, it can be divided into forward and backward part of each profile, as a result, the received signals are classified as "slow signals" and "fast signals", that is why in the 2-D simulation it turns out spectrum splitting phenomenon. However, for 3-D profiles, there is no distinct direction, so the simulation result turns out spectrum spreading phenomenon.

5. CONCLUSION

The "sea-spike" is a very special and important phenomenon in the research of electromagnetic scattering of sea surfaces. The multipath effects are introduced to explain this phenomenon. Different from the Bragg scattering mechanism, the multipath mechanism considers that some energy scatters directly back to the radar from the front face, while some scatters toward the front face of the wave and reflects toward the radar. In our research, the two typical breaking waves, the LONGTANK profiles and the measured plunging breaker, have been discussed after some treatments of aligning the 2-D profiles to the 3-D models. From the results under the numerical electromagnetic algorithm (MLFMA), the scattering characteristics in the breaking wave crests are presented both for the LONGTANK series and for the measured profiles. Meanwhile, the Doppler analysis for the plunging waves is also discussed, which associate with the evolution of this wave.

Compared with the 2-D profiles, the synthesized 3-D models are more likely true. Through the electromagnetic simulation in this paper, the "sea-spike" and Doppler shifts for two polarizations have been demonstrated, which are consistent with the conclusions of 2-D cases. However, there is a little difference between them, the Doppler frequency amplitude of 3-D models is higher than the 2-D case, as discussed in the Section 4. On the other hand, the effectiveness of the multilevel fast multipole algorithm (MLFMA) with adaptive higher order hierarchical Legendre basis functions has been validated in the analysis of breaking wave crests at the LGA.

ACKNOWLEDGMENT

This work was supported in part by the National High-Tech Research and Development Program of China (863 Program, No. 2007AA12Z159), supported by Chongqing Education Commission program (No. KJ100520).

REFERENCES

1. Ja, S. J., "Numerical study of microwave backscattering from breaking water waves," Ph.D. dissertation, Oklahoma State University, 1999.
2. West, J. C. and Z. Q. Zhao, "Electromagnetic modeling of multipath scattering from breaking water waves with rough faces," *IEEE Trans. Geosci.Remote Sens.*, Vol. 40, No. 3, 583–592, 2002.

3. West, J. C. and S. J. Ja, "Two-scale treatment of LGA scattering from spilling breaker water waves," *Radio Sci.*, Vol. 37, No. 4, 1054–1110, 2002.
4. Du, Y. and B. Liu, "A numerical method for electromagnetic scattering from dielectric rough surfaces based on the stochastic second degree method," *Progress In Electromagnetics Research*, Vol. 97, 327–342, 2009.
5. Wetzel, L. B., "Electromagnetic scattering from the sea at low grazing angles," *Surface Waves and Fluxes*, G. L. Geernaert and W. L. Plant (eds.), Vol. II, 109–171, Dordrecht, Kluwer, The Netherlands, 1990.
6. Trizna, D. B., "A model for Brewster angle damping and multipath effects on the microwave radar sea echo at low grazing angles," *IEEE Trans. Geosci. Remote Sens.*, Vol. 35, No. 5, 1232–1244, 1997.
7. West, J. C., "Low-grazing-angle (LGA) sea-spike backscattering from plunging breaker crests," *IEEE Trans. Geosci. Remote Sens.*, Vol. 40, No. 2, 523–526, 2002.
8. Plant, W. J., "A model for microwave doppler sea return at high incidence angles: Bragg scattering from bound, tilted waves," *J. Geophys. Res.*, Vol. 102, No. 21, 131–21, 146, 1997.
9. Ulaby, F. T., R. K. Moore, and A. K. Fung, *Microwave Remote Sensing: Active and Passive*, Artech House, Norwood, Massachusetts, 1986.
10. Bourlier, C., H. He, J. Chauveau, R. Hémon, and P. Pouliguen, "RCS of large bent waveguide ducts from a modal analysis combined with the Kirchhoff approximation," *Progress In Electromagnetics Research*, Vol. 88, 1–38, 2008.
11. Mittal, G. and D. Singh, "Critical Analysis of microwave specular scattering response on roughness parameter and moisture content for bare periodic rough surfaces and its retrieval," *Progress In Electromagnetics Research*, Vol. 100, 129–152, 2010.
12. Rice, S. O., "Reflection of electromagnetic wave from slightly rough surfaces," *Communications in Pure and Applied Mathematics*, Vol. 4, No. 2, 351–378, 1951.
13. Guo, L. X., Y. Liang, J. Li, and Z. S. Wu, "A high order integral spm for the conducting rough surface scattering with the tapered wave incidence-TE case," *Progress In Electromagnetics Research*, Vol. 114, 333–352, 2011.
14. Wright, J. W., "A new model for sea clutter," *IEEE Trans. Antennas Propag.*, Vol. 16, No. 2, 217–223, 1968.

15. Wu, Z. S., J. P. Zhang, L. X. Guo, and P. Zhou, "An improved two-scale model with volume scattering for the dynamic ocean surface," *Progress In Electromagnetics Research*, Vol. 89, 39–56, 2009.
16. Taboada, J. M., M. G. Araujo, J. M. Bertolo, L. Landesa, F. Obelleiro, and J. L. Rodriguez, "MLFMA-FFT parallel algorithm for the solution of large-scale problems in electromagnetics," *Progress In Electromagnetics Research*, Vol. 105, 15–30, 2010.
17. Song, J., C. C. Lu, and W. C. Chew, "Multilevel fast multipole algorithm for electromagnetic scattering by large complex objects," *IEEE Trans. Antennas Propag.*, Vol. 45, No. 10, 1488–1493, 1997.
18. Yang, W., Z. Zhao, C. Qi, W. Liu, and Z. P. Nie, "Iterative hybrid method for electromagnetic scattering from a 3-D object above a 2-D random dielectric rough surface," *Progress In Electromagnetics Research*, Vol. 117, 435–448, 2011.
19. Yang, W., Z. Q. Zhao, C. H. Qi, and Z. P. Nie, "Electromagnetic modeling of breaking waves at low grazing angles with adaptive higher order hierarchical legendre basis functions," *IEEE Trans. Geosci. Remote Sens.*, Vol. 49, No. 1, 346–352, 2011.
20. Wang, P., Y. Yao, and M. P. Tulin, "An efficient numerical tank for nonlinear water waves, based on the multi-subdomain approach with BEM," *Int. J. Numer. Meth. Fluids*, Vol. 20, No. 10, 1315–1336, 1995.
21. West, J. C., Z. Q. Zhao, X. N. Liu, and J. H. Duncan, "LGA scattering from measured breaking water waves: Extension to jetting surfaces," *IEEE 2001 International Geoscience and Remote Sensing Symposium, IGARSS'01*, Vol. 5, 2454–2456, 2001.
22. Li, Y. Z. and J. C. West, "Low-grazing-angle scattering from 3-D breaking water wave crests," *IEEE Trans. Geosci. Remote Sens.*, Vol. 44, No. 8, 2093–2101, 2006.
23. Thorsos, E. I., "The validity of the Kirchhoff approximation for rough surface scattering using a Gaussian roughness spectrum," *J. Acoust. Soc. Am.*, Vol. 83, No. 1, 78–92, 1988.
24. Zhao, Z. Q. and J. C. West, "Low-grazing-angle microwave scattering from a three-dimensional spilling breaker crest: A numerical investigation," *IEEE Trans. Geosci. Remote Sens.*, Vol. 43, No. 2, 286–294, 2005.
25. Haupt, R. L. and V. V. Liepa, "Synthesis of tapered resistive strips," *IEEE Trans. Antennas Propag.*, Vol. 35, No. 11, 1217–1225, 1987.